Sustainable Cities and Society 69 (2021) 102856

Contents lists available at ScienceDirect

Sustainable Cities and Society

journal homepage: www.elsevier.com/locate/scs

Stochastic energy management and scheduling of microgrids in correlated environment: A deep learning-oriented approach

Tan Cheng [a], Xiangqian Zhu [b,c,*], Xiaoyong Gu [a], Fan Yang [a], Mojtaba Mohammadi [d]

[a] School of Electrical and Control Engineering, Henan University of Urban Construction, Pingdingshan, 467036, China
[b] College of Building Environment Engineering, Zhengzhou University of Light Industry, Zhengzhou, 450002, China
[c] College of Electrical and Information Engineering, Hunan University, Changsha, 410082, China
[d] Department of Electrical Engineering, Shiraz University of Technology, Shiraz, Iran

ARTICLE INFO

Keywords:
Energy management
Cybersecurity
Hybrid microgrids
Long short-term memory
Prediction interval

ABSTRACT

Regarding the operation, reliability, security, and cost-effectiveness of microgrids (MGs), optimal energy management and data security are essential issues that must be taken into consideration. In this regard, this paper proposes a secured stochastic energy management scheme for both grid-connected and islanded hybrid AC-DC MGs (HMGs) considering renewable energy sources (RESs), plug-in hybrid electric vehicles (PHEVs), and energy storage devices (ESs). In this work, the operation of HMGs is formulated as a single objective optimization problem, which is solved using the interior search optimization algorithm (ISOA). In order to reinforce data security in HMGs, a deep learning-based intrusion detection system (IDS) based on the long short-term memory (LSTM) and prediction interval is proposed to detect false data injection attacks (FDIA) on advanced metering infrastructures (AMIs). In this work, the *2 m* point estimation method is utilized to model uncertainties associated with the forecasted output power of RESs, energy market price, charging demand of PHEVs, and load demand. The performance of the proposed scheme is evaluated using IEEE 33 bus test system for both operation modes.

1. Introduction

Smart grid, which is considered the future of electrical grids, is consisting several MGs at distribution level. Therefore, in order to achieve a cost-effective and reliable operation of smart grids, proper energy management of microgrids must be taken into account (Dabbaghjamanesh, Kavousi-Fard, Mehraeen, Zhang, & Dong, 2019). Generally, MGs can operate in two different modes: grid-connected and islanded. In grid-connected mode, MG is connected to the utility grid through the point of common coupling (PCC) and can exchange power with the utility grid based on costs and benefits. On the other hand, islanded MGs are not connected to the utility grid and must supply loads using only distributed generation (DG) units and ESs, which makes their management more challenging. From voltage-type point of view, there are three types of MGs: AC MGs, DC MGs, and hybrid AC-DC MGs. Since MGs are the last level of the electrical grid between utilities and end-users, there are several challenges associated with their energy management. For instance, new technologies such as ESs, PHEVs, RESs, etc. are connected to the grid through MGs and their implementation can cause serious challenges for MG's operators. For instance, PHEVs' sudden charging can impose unpredicted demand to the grid. Authors in (Papari, Edrington, Bhattacharya, & Radman, 2017), suggested a stochastic energy management scheme for HMGs based on crow search algorithm. In that paper, RESs and ESs are considered and the uncertain variables of the system are captured using unscented transform. In (Phommixay, Doumbia, & Qiushi, 2021), the *2 m* point estimation method is used to develop a stochastic management framework for MGs. Reference Gong et al. (2020), proposed a management scheme for HMGs considering plug-in electric vehicles, ESs, combine heat and power (CHP) model of fuel cells, RESs, and feeder reconfiguration strategy. Reference Dabbaghjamanesh, Kavousi-Fard, and Dong (2020), suggested a secured distributed cloud-fog based optimal scheduling framework for MGs. An energy management strategy for CHP-based MGs considering demand response technology and various generation units is proposed in (Perger, Wachter, Fleischhacker, & Auer, 2020). Reference Li, Rezvani, Hu, and Ohshima (2021) proposed a machine learning based energy management framework for optimal operation of hybrid MGs considering data security. A comprehensive review regarding the components and fundamentals of HMGs is presented in (Pourbehzadi et al., 2019). In that

* Corresponding author at: College of Building Environment Engineering, Zhengzhou University of Light Industry, Zhengzhou, 450002, China.
E-mail addresses: 30090102@hncj.edu.cn (T. Cheng), zhuxiangqian@zzuli.edu.cn (X. Zhu), 30010304@hncj.edu.cn (X. Gu), 30090504@hncj.edu.cn (F. Yang), mojtabamohammadi304@gmail.com (M. Mohammadi).

https://doi.org/10.1016/j.scs.2021.102856
Received 23 January 2021; Received in revised form 2 March 2021; Accepted 15 March 2021
Available online 20 March 2021

Nomenclature

B^t_{Gi}/ B^t_{si} DG/battery generation/storage cost
B^t_{Grid} Upstream grid power cost
b_i, b_f, b_o, b_h, … Bias vectors
c_t Cell state
C_{bat} PHEV battery capacity
DR_i/UR_i Ramp rate constraint of the DGs
f_t Forget gate
f Objective function in ISOA
$h(X)$ Cost objective function of the HMG
i_t Input gate at time t
N_T Number of time intervals
N_d/ $N_{d\text{-}DC}$/ $N_{d\text{-}AC}$ Number of DGs in the MG/DC sub-grid/AC sub-grid
$N_s/N_{s\text{-}DC}$ Number of ESs in the grid/DC sub grid
$N_{Load\text{-}DC}$ Loads in DC sub-grid
$NFE_{l,i}$ Normalize forecast error of ith smart meter at time t
N_b Number of busses in the grid
o_t Output gate
N_s/ $N_{s\text{-}DC}$ Number of batteries in MG/DC sub-grid
N_{Load} Number of loads in the MG
$P^t_{Grid,min}$/ $P^t_{Grid,max}$ Minimum/maximum power of the upstream grid
$P_{load\text{-}DC}$ loads in the DC sub-grid
$P^{inj,t}{}_j$/ $Q^{inj,t}{}_j$ Active/reactive power injected to the busses in the grid
P^{min}_{Gi}/ P^{max}_{Gi} Min/max output power of the ith DG unit
$P_{lm}i/P^i_{lf}$ Received/forecasted load value related to the ith smart meter
P^{min}_{conv}/ P^{max}_{conv} Min/max output power of the converter
P^t_{loss} Total power loss in the grid
$P^{line,t}_{i,max}$ Feeders' capacity
P^t_{Grid} power purchased/sold from/to the upstream grid
$P_{Loss\text{-}DC}$ Power loss in DC sub-grid
$P_{charge/discharge}$ permitted charge/discharge rate within a definite period of time Δt
$P_{charge/discharge,max}$ Maximum value of charging/discharging rate within a defined period of time Δt
P^t_{si}/ P^t_{Gi} Power of batteries/DGs
P_{PHEV} PHEV charger rate
r_1, r_2, r_3 randomly chosen value between 0 and 1
r_n A normally distributed vector of random numbers with the same size as x.
RES^t The value of spinning reserve
S^{on}_{Gi}/S^{off}_{Gi} DG units' Startup/shutdown cost
S^{on}_{sj}/S^{off}_{sj} Batteries' Startup/shutdown cost
t_{start} Charging Start time of the PHEV
t_D PHEV charging duration
u^t_i ON/OFF Status of the ith DG/battery
U_B/ L_B UPPER/lower bounds of the search space in ISOA
V^i_{min}/V^i_{max} Bus voltage limitations
V/δ Magnitude/phase of the voltage
W^t_{ess} battery energy storage
$W_{ess,max/min}$ Battery capacity
$W_{f,x}$, $W_{i,x}$, $W_{o,h}$,… Weighting matrices
X Control variables
x^j_{gb} global best in ISOA
Y/Θ line impedance magnitude/phase
y_t Output of the LSTM cell at time t
z Uncertain variable
$\eta_{charge/discharge}$ Charging/discharging efficiency of battery
η_{PHEV} PHEV charger efficiency
σ Logistic sigmoid function
σ^t_i/μ^t_i Mean/Standard deviation of the normal distribution function fitted on the NFEs of the n previous data in the proposed IDS
γ Coefficient of the proposed IDS

paper, stochastic mathematical model of RESs, operational zones, optimization schemes, load flow calculation methods, and control strategies are presented. A stochastic energy policy framework for smart MGs is proposed in (Hossain, Chakrabortty, Ryan, & Pota, 2020). In that paper, various generation units are considered and uncertainties in the system are captured using the unscented transform.

While most of the literature, are focused on the physical side of MGs, cybersecurity in these systems is overlooked. In the following, several works related to data security in MGs are presented. In reference Abdollah, Su, and Jin (2020), a machine learning-based intrusion detection system is proposed to detect integrity attacks on AMIs. Authors in (Ur-Rehman, Zivic, & Ruland, 2015) investigated cybersecurity in AMIs and suggested several countermeasures. Reference Jokar, Arianpoo, and Leung (2016) is focused on energy theft cyber-attacks. That paper utilized the transformer meters and proposed a detection scheme to detect abnormalities in loads' consumption patterns. Authors in (He, Mendis, & Wei, 2017) focused on the FDIAs on the state vector estimators and proposed a deep learning methodology to detect such attacks. Authors in (Kavousi-Fard, Dabbaghjamanesh, Jin, Su, & Roustaei, 2020), introduced a cyber-attack detection scheme based on the support vector machine and wavelet transform to detect flood cyber-attacks on electric vehicles' CAN bus. An overview of various types of metering systems in smart grids is presented in (Subhash & Rajagopal, 2014). In literature (Mehra, Dehalwar, & Kolhe, 2013), a two-level method is introduced to improve data communication security in AMIs. This method uses a dedicated authentication server to prevent unauthorized nodes to gain access to the system. Authors in (Ho, Wright, & Das, 2011), proposed a zone-based detection method based on the sequential probability ratio test to detect compromised zones in wireless sensor networks.

While the above works addressed significant aspects of operation and security of MGs, research in this area, especially data security, is still infancy. To address the first issue, in this work, a stochastic energy management scheme for optimal scheduling of HMGs is proposed. In this work, the interior search optimization algorithm (Gandomi, 2014), which is known as a powerful optimization tool, is utilized to solve the operation problem of the system and achieve the best solution. In case of PHEVs, three charging patterns (i.e. uncoordinated, coordinated, and smart charging) are considered to model various charging behaviors of PHEVs. Regarding the vital role of data security in the operation of modern power systems, in this paper, a deep learning-based IDS is proposed to detect FDIA on AMIs within MGs. The proposed IDS detects FDIAs on the loads' measured power demand based on a comparison between received data and corresponding data forecasted using LSTM. In order to model uncertainties in the system, the *2 m* point estimation method is utilized. The performance of the proposed scheme is examined using a modified IEE 33-bus test system. The simulation is performed for both operation modes. The main contribution of this paper is as follows:

- Proposing an optimal scheduling framework for the management of the hybrid AC-DC MGs considering PHEVs.
- Proposing a novel deep learning-based IDS for AMIs.
- Using the 2 m point estimation method to capture uncertainties in the HMG and utilizing ISOA to solve the operation problem of the SYSTEM.

The remainder of this paper is as below: section II presents the mathematical model of HMG and various charging patterns of PHEVs.

The ISOA is explained in section III. The basic theory of the 2 m point estimation method is presented in section IV. Section V is devoted to the deep learning-based IDS. Numerical simulation results are presented in section VI and the conclusion can be found in section VII.

2. Smart hybrid AC-DC microgrid

HMG is a cyber-physical system that incorporates various technologies. A schematic structure of the HMG's physical layer is presented in Fig. 1. In smart HMGs, the information related to the physical layer, such as active power, reactive power, voltage, etc. are reported to HMG central control using AMI in regular time intervals. In these systems, each node in the system is equipped with a smart metering device that communicates with HMG central control through communication channels. In the case of one day ahead operation, HMG central control schedules the system based on the system characteristics and forecasted values (i.e. predicted output power of renewable sources, energy market price, load demand). In the following, the operation of HMGs is formulated as a constraint optimization problem, and also different charging behaviors of PHEVs are presented.

2.1. Problem formulation and limitations

The cost objective function of the HMG incorporates various costs in the grid as follows:

$$\begin{aligned} Min\ h(X) = \sum_{t=1}^{N_T}\Big(\sum_{i=1}^{N_g}[u_i^t P_{Gi}^t B_{Gi}^t + S_{Gi}^{on}\max\{0, u_i^t - u_i^{t-1}\}+ \\ +S_{Gi}^{off}\max\{0, u_i^{t-1} - u_i^t\}] + \sum_{j=1}^{N_S}[u_j^t P_{sj}^t B_{sj}^t + S_{sj}^{on}\max\{0, u_j^t - u_j^{t-1}\}+ \\ +S_{sj}^{off}\max\{0, u_j^{t-1} - u_j^t\}] + P_{Grid}^t B_{Grid}^t\Big) \end{aligned} \tag{1}$$

Where X presents the control variables as follows:

$$\begin{aligned} X = [P_g, U_g]_{1\times(2\times n\times N_T)}, \quad n = N_d + N_s + 1; \quad \forall t \in N_T \\ P_g^t = [P_G^t, P_s^t, P_{Grid}^t]; \quad P_G^t = [P_{G1}^t, P_{G2}^t, ..., P_{GN_g}^t] \\ U_g^t = [u_1^t, u_2^t, ..., u_{N_d}^t]; \quad P_s^t = [P_{s1}^t, P_{s2}^t, ..., P_{sN_s}^t] \\ P_{Grid}^t = [P_{Grid}^t], \quad u_k^t \in \{0, 1\} \end{aligned} \tag{2}$$

Note that in islanded mode the cost of the upstream grid (i.e. P^t_{Grid}) is zero. The cost objective function is optimized considering several practical and technical limitations. Eqs. (3)–(5) shows the power balance in the DC and AC sub-grids.

$$\sum_{i=1}^{N_{d-DC}} P_{Gi}^t + P_{conv}^t + \sum_{j=1}^{N_{s-DC}} P_{sj}^t = \sum_{k=1}^{N_{Load-DC}} P_{Load-DC}^t + P_{Loss-DC} \tag{3}$$

$$P_j^{inj,t} = \sum_{n=1}^{N_b} V_j^t V_n^t Y_{jn}\cos(\theta_{jn} + \delta_j - \delta_n) \tag{4}$$

$$Q_j^{inj,t} = \sum_{n=1}^{N_b} V_j^t V_n^t Y_{jn}\sin(\theta_{jn} + \delta_j - \delta_n) \tag{5}$$

In the following the rest of the limitations are presented:

- utility grid and DGs capacity constraint:

$$\begin{aligned} P_{Gi,\min}^t \le P_{Gi}^t \le P_{Gi,\max}^t \\ P_{conv,\min}^t \le P_{conv}^t \le P_{conv,\max}^t \\ P_{Grid,\min}^t \le P_{Grid}^t \le P_{Grid,\max}^t \end{aligned} \tag{6}$$

- spinning reserve:

$$\sum_{i=1}^{N_d} u_i^t P_{Gi,\max}^t + P_{Grid,\max}^t \ge \sum_{k=1}^{N_{Load}} P_{Load,k}^t + P_{loss}^t + \mathrm{Res}^t \tag{7}$$

- feeder capacity constraint:

$$\left|P_i^{Line,t}\right| \le P_{i,\max}^{Line} \tag{8}$$

- bus voltage constraint:

$$V_m^{\min} \le V_m^t \le V_m^{\max} \tag{9}$$

- ramp-rate constraint:

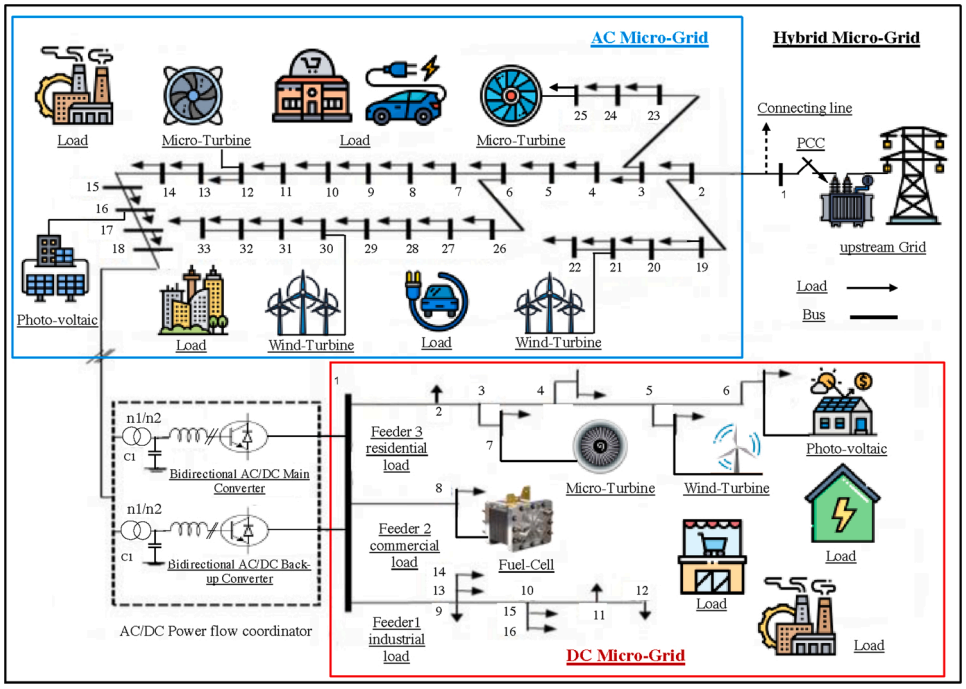

Fig. 1. Schematic illustration of HMG's physical layer.

$$\left|P_{Gi}^{t}-P_{Gi}^{t-1}\right|<UR_i,DR_i \tag{10}$$

- ES constraints:

$$W_{ess}^{t}=W_{ess}^{t-1}+\eta_{charge}P_{charge}\Delta t-\frac{1}{\eta_{discharge}}P_{discharge}\Delta t \tag{11}$$

$$\begin{cases} W^{ess,\min}\le W_{ess}^{t}\le W^{ess,\max} \\ P_{charge,t}\le P_{charge,\max} \\ P_{discharge,t}\le P_{discharge,\max} \end{cases} \tag{12}$$

2.2. Charging behavior of PHEVs

Generally, there are three types of electric vehicles: plug-in electric vehicles, hybrid electric vehicles, and PHEVs (Rostami, Kavousi-Fard, & Niknam, 2015). The main focus of this paper is on PHEVs. In this work three charging patterns for PHEVs (i.e. uncoordinated, coordinated, and smart charging) is considered. It is worth noting that in this work, the PHEV-20 is considered as the base case. In the uncoordinated strategy, there is no limitation on the charging behavior of PHEVs. The charging start time of PHEVs in the uncoordinated scenario is obtained using a uniformly distributed probability density (PDF) as follows:

$$f(t_{start})=\frac{1}{b-a}\quad a\le t_{start}\le b\quad a=18,b=19 \tag{13}$$

In the second strategy (i.e. coordinated), the PHEV owners are willing to charge their vehicles in low-demand hours especially after 9:00 p.m. The charging start time of PHEVs in the second strategy is achieved using a uniformly distributed PDF as follows:

$$f(t_{start})=\frac{1}{b-a}\quad a\le t_{start}\le b\quad a=21,b=24 \tag{14}$$

In the third charging strategy (i.e. smart), the policy is to minimize the cost for both utilities and consumers. Therefore, in this scenario, the most optimum charging pattern for PHEVs is considered. In order to model the charging behavior of PHEVs in this scenario, a normal PDF is considered as follows:

$$f(t_{start})=\frac{1}{\sigma\sqrt{2\pi}}e^{\left(-\frac{1}{2}\left(\frac{t_{start}-\mu}{\sigma}\right)^2\right)}\quad \mu=1,\sigma=3 \tag{15}$$

The PEVs' battery state of charge (SOC), the driven mile per day of the PHEVs, the charging duration of PHEVs, and PHEVs' battery capacity PDF characteristics are obtained using the following equations respectively:

$$SOC=\begin{cases} 0 & m>AER \\ \dfrac{AER-m}{AER}\times 100\% & m\le AER \end{cases} \tag{16}$$

$$f_m(m)=\frac{1}{m\sigma\sqrt{2\pi}}e^{\frac{-(\ln(m)-\mu)^2}{2\sigma^2}}\quad m>0 \tag{17}$$

$$t_D=\frac{C_{bat}\times(1-SOC)\times DOD}{\eta_{PHEV}\times P_{PHEV}} \tag{18}$$

$$\begin{aligned} \mu_{C_{bat}}&=\frac{MinC_{bat}+MaxC_{bat}}{2} \\ \sigma_{C_{bat}}&=\frac{MaxC_{bat}-MinC_{bat}}{4} \end{aligned} \tag{19}$$

Where AER stands for the all-electric range of PHEVS and DOD stands for the depth of discharge. Complete information related to the charger characteristics, market share and battery capacity of PHEV types can be found in (Rostami et al., 2015).

3. Interior search optimization algorithm

In this work, the ISOA is utilized to solve the proposed optimization problem. The ISOA is a metaheuristic optimization algorithm that models the interior design and decoration process (Gandomi, 2014). The best solution in the interior design process can be defined as producing an interior space that meets the requirements, goals, and constraints and also satisfies the client. In the ISOA, the components are divided into two different groups called the composition group and the mirror group. In the first group, the combination of components is dynamically modified to find the best view. On the other hand, in the mirror group, better views are found by placing a mirror between the components and the fittest element. The ISOA solves the optimization problem based on the following steps:

- *Step 1:* upper (U_B) and lower (L_B) bounds of the search space are specified and random locations for components within the search space are generated.
- *Step 2:* using the cost objective function, the best solution is specified. This component is considered the global best (x_{gb}^{j}).
- *Step 3:* other components are randomly categorized in one of the groups (i.e. mirror group or composition group). For this purpose, variable (μ), which is in the range of [0,1] is considered. If $\mu\le r_1$, the component goes to the composition group. Otherwise, it goes to the mirror group. Since the (μ) is the only parameter of the ISOA, it must be adjusted carefully.
- *Step 4:* the position of components in the composition group are randomly changed based on the following equation:

$$x_i^j=LB^j+\left(UB^j-LB^j\right)\times r_2 \tag{20}$$

U_B^j and L_B^j, which are the maximum and minimum values of the j-1^{th} iteration, are considered as the upper and lower bounds in the j^{th} iteration.

- *step 5:* a mirror is placed between each component in the mirror group and the best solution in the search space as follows:

$$x_{i,m}^j=r_3\times x_{i,m}^{j-1}+(1-r_3)\times x_{gb}^j \tag{21}$$

The position of the image of the component is calculated as follows:

$$x_i^j=2\times x_{m,i}^j-x_i^{j-1} \tag{22}$$

- *Step 6:* in order to achieve better solutions, in each iteration, the position of the global best is slightly changed using the following equation:

$$\begin{cases} x_{gb}^j=x_{gb}^{j-1}+r_n\times\zeta \\ \xi=0.01\times(U_B-L_B) \end{cases} \tag{23}$$

- *Step 7:* the fitness function of the components and their images in the mirror is calculated and then their location is updated as follows:

$$x_{gb}^j=\begin{cases} x_i^j & f(x_i^j)<f(x_i^{j-1}) \\ x_i^{j-1} & o.w \end{cases} \tag{24}$$

- *Step 8:* if the iteration criterion is not reached, the process goes to step 2 and starts again.

4. *2m* point estimation stochastic method

Regarding the high level of uncertainties in the system, a proper stochastic modeling technique is required to model uncertainties. In this section, the basic theory of the *2 m* point estimation method is presented. In this work, the *2m* point estimation method is utilized to model

uncertainties associated with forecasted output power of RESs, energy market price, charging demand of PHEVs, and load demand. Generally, there are three types of stochastic modeling methods: 1) Monte-Carlo simulation method, 2) Analytical models, and 3) approximation methods. *2m* point estimation method, which is an approximation method, is the improved version of the classic point estimation method (Phommixay et al., 2021). In this method, uncertain variables are replaced by two different points on both sides of the mean value in the corresponding distribution function. Afterward, the problem is solved *2m* times. Each time using one of the points where other uncertain variables are fixed. The mathematical description of the process is presented as follows:

$$S = F(z) \tag{25}$$

$$z = [z_1, z_2, \ldots, z_m] \tag{26}$$

A probability function f_l is considered for each uncertain variable z_l to model uncertainties. The *2 m* point estimation method utilizes the mean value, standard deviation, and skewness of the f_l as its main characteristics, to replace it with two concentrations. Therefore, (25) is solved *2 m* times when there are *m* uncertain variables in the system. Fig. 2 shows the graphical illustration of the *2 m* point estimation method. As it can be seen from Fig. 2, two points ($z_{l,1}$ and $z_{l,2}$), which are located on both sides of the mean value, are mapped to the output data $S_{l,1}$ and $S_{l,2}$. Note that $W_{l,1}$ and $W_{l,2}$ are weighting factors. Basically, for any concentration point two pair of points are computed. The value of the $z_{l,k}$, standard deviation of the $f_{l,k}$, and other parameters of the method are obtained as follows:

$$z_{l,k} = \mu_{z_l} + \xi_{l,k}.\sigma_{z_l}; k = 1, 2 \tag{27}$$

$$\xi_{l,k} = \frac{\lambda_{l,3}}{2} + (-1)^{3-k}\sqrt{n - \left(\lambda_{l,3}^2/2\right)^2}, \quad k = 1,\ 2 \tag{28}$$

$$\lambda^{l,3} = \frac{E\left[\left(z_l - \mu_{z_l}\right)^3\right]}{\left(\sigma_{z_l}\right)^3} \tag{29}$$

$$\sigma = \sqrt{\mathrm{var}(S_i)} = \sqrt{E(S_i^2) - [E(S_i)]^2} \tag{30}$$

Note that in (30) the operator *E* presents the expected value.

5. The deep learning-based intrusion detection system

In this section, an IDS based on LSTM is proposed to detect FDIA against load smart meters in HMGs. In the proposed IDS, first, the load demand is predicted using LSTM and then the normalized forecast error (NFE) is compared with a certain bound called the prediction interval, and a decision is made. After new data is received, a normal distribution function is fitted on the NFEs of *n* previous received data. If the NFE of the received data lies outside of the prediction interval, the received data is considered as the attack, and if the NFE of the received data lies inside, the received data is considered legitimate.

$$NFE_{l,i} = \left(\left(P^i_{l,m} - P^i_{l,f}\right)\Big/ P^i_{l,f}\right)$$

$$Decision: \begin{cases} Attack & o.w \\ No-attack & \mu_i^t - \gamma \times \sigma_i^t < NEF_{l,i} < \mu_i^t + \gamma \times \sigma_i^t \end{cases} \tag{31}$$

The value of γ indicates the width of the prediction interval and confidence level such that higher values of γ causes wider prediction intervals. The value of γ and *n*, which are considered as the model's hyper parameters, is determined by the system operators based on their desired confidence level. In the following, the LSTM that is utilized for load forecasting is explained in detail.

Fig. 3 shows the normal distribution function and different prediction intervals considering different values of γ. As can be seen from that figure, higher values of γ result in wider intervals.

5.1. The long short term memory

Generally, the LSTM is proposed as a solution to the gradient vanishing problem in conventional recurrent neural networks (Hochreiter & Schmidhuber, 1997). The LSTM makes use of the cell state and three cell gates to record and hold the information. The input gate and forget gate specify the information that should be added to the cell state and removed from the cell state respectively. Also, the output gate specifies which part of the cell state must be used in the output. The structure of the LSTM cell is illustrated in Fig. 4. Note that the training process in the LSTM network is carried out using the backpropagation process (Werbos, 1990). The transition equations of the LSTM is described as follows:

$$h_t = H(W_{x,h}x_t + W_{h,h}h_{t-1} + b_h) \tag{32}$$

$$y_t = W_{h,y}h_t + b_y \tag{33}$$

The function H is implemented as follows:

$$i_t = \partial(W_{i,x}x_t + W_{i,h}h_{t-1} + b_i) \tag{34}$$

$$f_t = \partial(W_{f,x}x_t + W_{f,h}h_{t-1} + b_f) \tag{35}$$

$$\overline{c_t} = \tanh(W_{\overline{c},x}x_t + W_{\overline{c},x}h_{t-1} + b_{\overline{c}}) \tag{36}$$

$$o_t = \partial(W_{o,x}x_t + W_{o,h}h_{t-1} + b_o) \tag{37}$$

$$C_t = f_t \cdot c_{t-1} + i_t \cdot \overline{c}_t \tag{38}$$

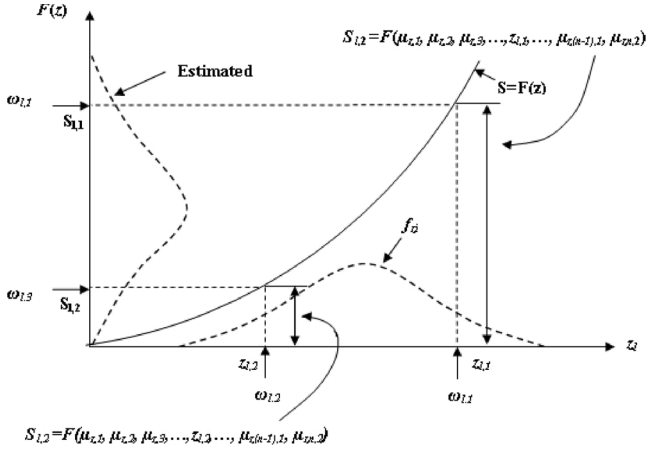

Fig. 2. Graphical illustration of the 2*m* point estimation method.

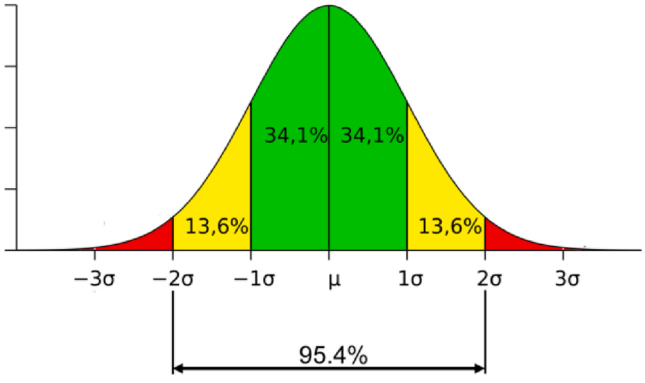

Fig. 3. Normal Distribution Function considering different values of γ.

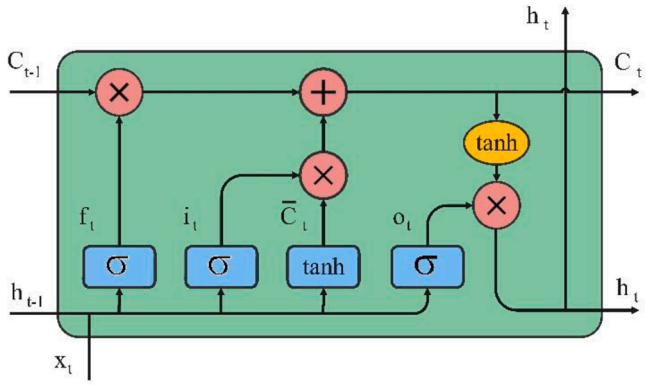

Fig. 4. Structure of LSTM cell.

$$h_t = o_t \cdot \tanh(c_t) \tag{39}$$

6. Numerical simulation results

This section is devoted to numerical simulation. In this section, the modified IEEE 33-bus test system is used to evaluate the performance of the proposed scheme. The schematic illustration of the test system can be found in Fig. 1. The test system includes several DG units, one ES, and 300 PHEVs with penetration level of %60. The characteristics of the DG units can be found in Table 1. The voltage levels in the AC and DC sub-grids are considered as 12.6 kV and 1 kV respectively. In this work, due to the high importance of green energy production, the RESs are considered as nondispatchable units. Note that in the simulations the line resistance in the DC sub-grid is neglected. Regarding the HMG's islanded mode, the point of common coupling is equipped with a circuit breaker that disconnects the HMG from the utility grid if necessary. Table 3 shows the normalized values of the forecasted output power of WTs and PVs, electricity market price, loads demand in DC sub-grids and the load factor in AC sub-grid. All WTs and PVs have the same generation pattern as Table 2. The results are provided considering five scenarios as follows:

- *Scenario 1*: HMG operates in grid-connected mode and PHEVs are not considered in the system.

Table 1
Specification of the test system.

Type	Min Power (kW)	Max Power (kW)	Bid ($/kWh)	Startup/ shutdown cost ($)	Ramp Up/ Down Rate	Bus Number
Micro-turbine 2	100	1300	0.675	75	220	12
Micro-turbine 3	90	1100	0.675	70	180	25
Wind-turbine 2	0	550	1.073	0	–	30
Wind-turbine 3	0	450	1.073	0	–	21
Photovoltaic 2	0	400	2.584	0	–	16
AC-DC converter	−1500	1500	–	–	–	18
Fuel cell	50	700	0.394	38.5	110	DC MG
Wind-turbine 1	0	200	1.073	0	–	DC MG
Micro-turbine 1	35	300	0.48	68	80	DC MG
Photovoltaic 1	0	250	2.584	0	–	DC MG
Energy storage	−350	350	0.318	0	–	DC MG

Table 2
Normalized output power of RESs, AC MG load factor, DC MG load demand, and market price.

hour	Market price ($/kWh)	WT normalized output power	PV normalized output power	AC MG load factor	DC MG load (Kw)
1	0.23	0.119	0	0.6	156
2	0.19	0.119	0	0.65	150
3	0.14	0.089	0	0.59	150
4	0.12	0.15	0	0.62	153
5	0.12	0.204	0	0.7	168
6	0.2	0.18	0	0.698	174
7	0.2	0.24	0.109	0.71	210
8	0.2	0.26	0.25	0.79	225
9	1.5	0.26	0.34	0.86	228
10	4	0.3	0.39	0.9	240
11	4	0.29	0.468	0.98	234
12	4	0.31	0.47	1	222
13	1.5	0.29	0.461	0.99	216
14	4	0.27	0.5	1	216
15	2	0.285	0.47	0.97	228
16	1.95	0.298	0.35	0.958	240
17	0.6	0.33	0.26	0.935	255
18	0.41	0.35	0.19	0.86	264
19	0.35	0.4	0.04	0.88	270
20	0.63	0.45	0	0.91	261
21	1.17	0.42	0	0.927	234
22	0.64	0.39	0	0.887	213
23	0.3	0.36	0	0.78	195
24	0.26	0.22	0	0.7	168

- *Scenario 2*: HMG operates in grid-connected mode and the uncoordinated charging strategy of PHEVs is considered.
- *Scenario 3*: HMG operates in grid-connected mode and the coordinated charging strategy of PHEVs is considered.
- *Scenario 4*: HMG operates in grid-connected operation mode and the smart charging strategy of PHEVs is considered.
- *Scenario 5*: HMG operates in an islanded mode and the smart charging strategy of PHEVs is considered.

As can be seen from Table 3, which presents the results of the scenarios, the highest total cost of the system in the grid-connected mode where PHEVs are considered is related to the uncoordinated charging strategy. On the other hand, the smart charging strategy has the lowest cost. These results indicate the high impact of PHEVs' charging strategy on the operation cost of the system. Table 4 illustrates the vital role of optimal scheduling in reducing the grid's total operation cost can be indicated such that at the early hours of the day that the energy market price is low, shutting down the expensive DG units and purchasing power from the utility grid can highly decrease the costs. Comparing the power loss of the HMG in different scenarios shows the impact of the local load supply on decreasing power loss of the system. It is worth noting that the maximum voltage deviation limitation (i.e. 0.1 pu) is satisfied in all scenarios. Due to more promising results related to the smart charging strategy, only the results of the smart charging strategy are discussed in the rest.

Table 3
Comparison of different operation scenarios.

Operation Mode	PHEV Charging Type	Power Loss (kW)	Total Cost ($)	Maximum Voltage Deviation (pu)
Islanded	Smart	2588	60049	0.04
Grid-connected	No-PHEV	2766	50843	0.09
	Uncoordinated	2810	57931	0.08
	Coordinated	2777	53140	0.08
	Smart	2866	51505	0.08

Table 4
Optimal scheduling of the test system in the grid-connected operation mode considering smart charging strategy for PHEVs.

Hour	PV1	WT1	Fuel Cell	MT1	AC-DC Converter	MT2	MT3	WT2	WT3	PV2	Enegy Storage
1	0	24.5	0	0	482.2	0	0	67.38	55.13	0	−350
2	0	23.05	0	35	441.2	0	0	63.4	51.87	0	−350
3	0	17.78	57.45	0	424.75	0	0	48.9	40.01	0	−350
4	0	29.84	50	37.96	385.036	0	0	82.05	67.13	0	−350
5	0	41.4	65.75	78.56	312.683	0	0	113.8	93.14	0	−329.8
6	0	36.75	166.6	39.05	281.923	0	179.6	101.1	82.7	0	−349.5
7	27.94	49.22	255.4	47.91	135.214	220	359.5	135.4	110.8	44.71	−303.8
8	61.1	50.84	365.2	125.9	−66.4907	440	535.8	139.8	114.4	97.76	−314.1
9	86.53	52.93	473.8	205.6	−935.5	660	707.8	145.6	119.1	138.4	347.06
10	99.01	60.93	577.8	204.9	−1042.48	880	884.4	167.6	137.1	158.4	342.33
11	113.1	56.04	603.5	196	−1090.11	932.6	1050	154.1	126.1	180.9	349.62
12	113	59.64	595.5	131.6	−890.095	1136	1100	164	134.2	180.8	205.49
13	115.2	57.99	599.6	70.09	−893.843	1109	1098	159.5	130.5	184.4	266.92
14	130.7	56.48	686.8	72.64	−756.926	1300	1100	155.3	127.1	209.2	34.512
15	115.6	56.09	698.4	133.8	−702.425	1267	1071	154.2	126.2	185	−76.27
16	88.25	60.11	692.9	66.89	−998.997	1101	932.8	165.3	135.2	141.2	332.05
17	63.2	64.18	696.9	0	−922.93	890.3	840.3	176.5	144.4	101.1	350
18	48.69	71.76	640.5	80	−496.661	670.4	674.9	197.3	161.5	77.91	−77.36
19	9.755	78.04	561.8	84.52	−116.369	844	718.7	214.6	175.6	15.61	−350
20	0	90.05	625.2	164.5	−903.384	993.9	611.9	247.6	202.6	0	284.7
21	0	85.67	700	244.5	−1144.52	1207	569.8	235.6	192.8	0	350
22	0	81.05	700	272.2	−1175.4	1114	468	222.9	182.4	0	338.18
23	0	75.31	590	215.1	−332.145	951.8	300.3	207.1	169.4	0	−350
24	0	44.21	498.2	146.8	−178.238	903.3	152.8	121.6	99.47	0	−342.7

6.1. Optimal scheduling of HMG

This part is devoted to the optimal scheduling of the HMG for both operation modes considering the smart charging strategy of PHEVs.

6.1.1. Optimal scheduling of the grid-connected HMG

Table 4 shows the optimal output power of DG units, ES, and converter in the grid-connected HMG. According to this table and Table 2, at the early hours of the day, that energy market fee is low, dispatchable units are turned off and most of the loads are supplied by the utility grid. By comparing the total operation cost of the system in this scenario with the islanded mode where there is no utility grid, it can be concluded that this is a beneficial policy. Similarly, it can be seen that at the peak load hours (middle of the day), which the market price is high, all DGs are operating near their maximum generation capacity to avoid purchasing expensive electricity from the utility grid. Since the power generation capacity of DG units in the DC part is more than its load demand, DC sub-grid injects power to the AC sub-grid at peak load hours and helps the system to decrease the operation cost. In the case of ES, according to Table 4, it can be seen that at the early hours of the day that energy market price is low, the ES stores the energy and injects its stored energy into the grid at peak load hours (high market price hours). Therefore, the presence of the ESs in the grid is efficient. Note that negative power values of ESs are related to the power discharge.

6.1.2. Optimal scheduling of the islanded HMG

Details of the optimal scheduling of the system for islanded operation mode can be found in Table 5. As can be seen, due to the lack of a utility

Table 5
Optimal scheduling of the test system in the islanded operation mode.

Hour	PV1	WT1	Fuel Cell	MT1	AC-DC Converter	MT2	MT3	WT2	WT3	PV2	Energy Storage
1	0	24.5	479.8	117.1	−114.703	1300	1100	67.38	55.13	0	−350
2	0	23.05	550.4	135.1	−394.489	1300	1100	63.4	51.87	0	−164.8
3	0	17.78	539.4	55.14	−112.583	1300	1100	48.9	40.01	0	−349.7
4	0	29.84	592.5	133.4	−279.02	1300	1100	82.05	67.13	0	−323.9
5	0	41.4	686	55.39	−398.688	1300	1100	113.8	93.14	0	−215.6
6	0	36.75	642.6	135.4	−323.741	1300	1100	101.1	82.7	0	−316.3
7	27.94	49.22	700	145.3	−518.239	1300	1100	135.4	110.8	44.71	−192.3
8	61.1	50.84	664	122.2	−509.845	1300	1100	139.8	114.4	97.76	−165.8
9	86.53	52.93	554	142.1	−422.021	1300	1100	145.6	119.1	138.4	−183.1
10	99.01	60.93	444	171.3	−720.865	1293	924.4	167.6	137.1	158.4	188.12
11	113.1	56.04	477.9	219.5	−831.976	1300	1100	154.1	126.1	180.9	193.55
12	113	59.64	587.9	220.8	−892.877	1300	1100	164	134.2	180.8	126.68
13	115.2	57.99	498.4	147.9	−877.225	1300	1100	159.5	130.5	184.4	273.71
14	130.7	56.48	567	71.19	−927.152	1300	1100	155.3	127.1	209.2	325.96
15	115.6	56.09	508.9	133.4	−797.513	1300	1097	154.2	126.2	185	208.76
16	88.25	60.11	614.2	128.7	−944.571	1300	952.7	165.3	135.2	141.2	294.57
17	63.2	64.18	671.7	208.7	−822.097	1265	1007	176.5	144.4	101.1	65.674
18	48.69	71.76	571.9	242.7	−793.92	1191	827.6	197.3	161.5	77.91	125.84
19	9.755	78.04	637.9	293.3	−721.71	1300	868.7	214.6	175.6	15.61	−29.43
20	0	90.05	699.1	293.4	−901.608	1300	783.5	247.6	202.6	0	80.201
21	0	85.67	692.7	345.9	−884.627	1300	892.2	235.6	192.8	0	−4.021
22	0	81.05	582.7	327.4	−954.131	1300	712.6	222.9	182.4	0	178.99
23	0	75.31	663.4	324.2	−672.775	1265	630.1	207.1	169.4	0	−191.8
24	0	44.21	553.4	338	−621.702	1221	563.6	121.6	99.47	0	−145.8

grid, DGs are operating near their maximum capacity and all loads are supplied only by DGs. According to Table 3, in comparison with grid-connected mode, which HMG can exchange power with the utility grid, the operation cost of the islanded HMG is higher. This shows that in terms of cost reduction, the flexibility of the system in islanded mode is lower than grid-connected. Since in smart charging strategy the most beneficial charging pattern is considered, most PHEVs are charged at the beginning of the day in which energy demand is low. Despite the low power demand at the beginning of the day, this policy results in high demand at these hours. As a result, in addition to the peak-load hours, the power flow in the converter is toward the AC sub-grid at all hours. According to Table 5, the ES is charged at the beginning of the day, which power demand is low, and is discharged at peak load hours. This policy helps to keep the operation cost of the system as low as possible.

6.2. The deep learning-based IDS performance examination

This section is devoted to the examination of the proposed IDS using a practical test case. To this end, the hourly load data of the power supply company of Johor city in Malaysia (Sadaei et al., 2019) is utilized to examine the performance of the proposed IDS. In this regard, 15 months of the hourly load data from 01/01/2009 to 14/03/2010 is utilized to train the network and then 3.5 months of data from 15/03/2010 to 02/07/2010 is used as the test data. The LSTM network includes two 128-cell layers, one dropout layer with 0.3 rate, and one fully connected output layer. It is worth noting that the network is trained considering a 14 -h time lag window, Adam as optimizer, and 150 epochs using Keras library in python 3.8. The results of the load prediction are compared with artificial neural networks (ANN). Different metrics of the trained networks (i.e. mean absolute percentage error (MAPE), mean absolute error (MAE), and root mean square error (RMSE)) are compared in Table 6. As can be seen from that table, the LSTM network has a much better performance such that the LSTM could reach 2.192 % MAPE where ANN has 4.152 %. This is due to deep structure of LSTM.

The regression diagram of both methods (i.e. LSTM and ANN) for a 48 -h interval from 19/03/2010-00:00 to 21/03/2010-23:00 is presented in Fig. 5. The good performance and priority of the proposed LSTM-based load forecasting method can be seen at the sharp points.

Now the network is trained, we use 5 days of load data received from 15/05/2010-13:00 to 20/05/2010-13:00 to test the effect of γ on the performance of the proposed IDS. In this scenario, the value of n is considered as *1440 (*two months). Fig. 6 shows the impact of γ on the true negative rate and the false-positive rate of the IDS. As can be seen from that figure, increasing γ increases the true negative rate, and decrease the false-positive rates. However, increasing γ reduces the sensitivity to the attack at the same time. Therefore, it can be concluded that there is a tradeoff between the performance of the proposed IDS and its sensitivity to attacks.

7. Conclusion

This paper proposed a secured stochastic energy management scheme for hybrid AC-DC microgrids considering WTs, PVs, PHEVs, and ESs. The operation of the system is formulated as a constrained optimization problem. In the proposed scheme the interior search algorithm used to solve the optimization problem of the system. Also in this work, three charging strategies for PHEVs were introduced and the *2 m* estimation method was utilized to capture the uncertainties in the system. The simulation results illustrated the vital role of PHEV charging strategy on the total operation cost of the HMG. Also, it was concluded that it is more beneficial to charge batteries at the first hours of the day and discharge them at peak load hours. To reinforce data security in the AMIs, this paper proposed an IDS based on the LSTM to detect FDIA in the grid. The performance of the LSTM was tested on a practical dataset and the results showed the priority of LSTM over ANN. Also, it concluded that there is a tradeoff between the sensitivity of the proposed IDS and the accuracy of the model. The tradeoff can be adjusted using the model's corresponding coefficient.

Table 6
Performance of the LSTM vs ANN.

	MAPE (%)	MAE (W)	RMSE (W)
LSTM	2.1928	931.63	1361.8
ANN	4.1529	1676.2	2258.8

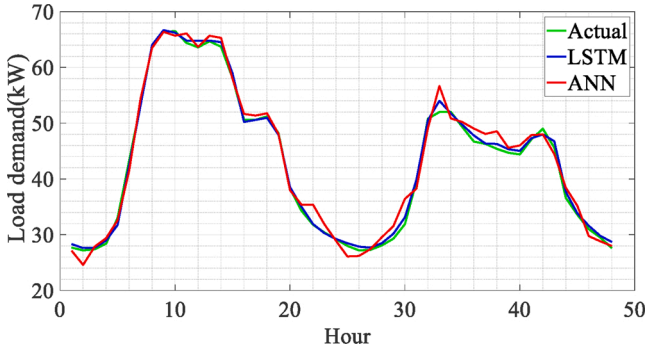

Fig. 5. Regression diagram of the LSTM and ANN vs actual load.

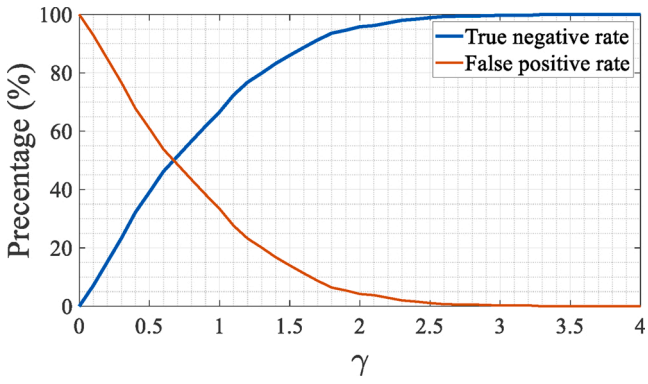

Fig. 6. Effect of γ on the true negative and false positive rate.

Declaration of Competing Interest

The authors report no declarations of interest.

References

Abdollah, K.-F., Su, W., & Jin, T. (2020). A machine learning based cyber attack detection model for wireless sensor networks in microgrids. *IEEE Transactions on Industrial Informatics*.

Dabbaghjamanesh, M., Kavousi-Fard, A., Mehraeen, S., Zhang, J., & Dong, Z. Y. (2019). Sensitivity analysis of renewable energy integration on stochastic energy management of automated reconfigurable hybrid AC–DC microgrid considering DLR security constraint. *IEEE Transactions on Industrial Informatics, 16*(1), 120–131.

Dabbaghjamanesh, M., Kavousi-Fard, A., & Dong, Z. (2020). A novel distributed cloud-fog based framework for energy management of networked microgrids. *IEEE Transactions on Power Systems*.

Gandomi, A. H. (2014). Interior search algorithm (ISA): A novel approach for global optimization. *ISA Transactions, 53*(July (4)), 1168–1183.

Gong, Xuan, Dong, Feifei, Mohamed, Mohamed A., Abdalla, Omer M., & Ziad Ali, M. (2020). A secured energy management architecture for smart hybrid microgrids considering PEM-fuel cell and electric vehicles. *IEEE Access, 8*, 47807–47823.

He, Y., Mendis, G. J., & Wei, J. (2017). Real-time detection of false data injection attacks in smart grid: A deep learning-based intelligent mechanism. *IEEE Transactions on Smart Grid, 8*(5), 2505–2516.

Ho, J.-W., Wright, M., & Das, S. K. (2011). ZoneTrust: Fast zone-based node compromise detection and revocation in wireless sensor networks using sequential hypothesis testing. *IEEE Transactions on Dependable and Secure Computing, 9*(4), 494–511.

Hochreiter, S., & Schmidhuber, J. (1997). Long short-term memory. *Neural Computation, 9*(8), 1735–1780.

Hossain, M. A., Chakrabortty, R. K., Ryan, M. J., & Pota, H. R. (2020). Energy management of community energy storage in grid-connected microgrid under uncertain real-time prices. *Sustainable Cities and Society*, Article 102658.

Jokar, P., Arianpoo, N., & Leung, V. C. M. (2016). Electricity theft detection in AMI using customers' consumption patterns. *IEEE Transactions on Smart Grid, 7*(Jan. (1)), 216–226. https://doi.org/10.1109/TSG.2015.2425222

Kavousi-Fard, A., Dabbaghjamanesh, M., Jin, T., Su, W., & Roustaei, M. (2020). An evolutionary deep learning-based anomaly detection model for securing vehicles. *IEEE Transactions on Intelligent Transportation Systems*.

Li, H., Rezvani, A., Hu, J., & Ohshima, K. (2021). Optimal day-ahead scheduling of microgrid with hybrid electric vehicles using MSFLA algorithm considering control strategies. *Sustainable Cities and Society, 66*.

Mehra, T., Dehalwar, V., & Kolhe, M. (2013). Data communication security of advanced metering infrastructure in smart grid. September. In *2013 5th International Conference and Computational Intelligence and Communication Networks* (pp. 394–399).

Papari, B., Edrington, C. S., Bhattacharya, I., & Radman, G. (2017). Effective energy management of hybrid AC–DC microgrids with storage devices. *IEEE Transactions on Smart Grid, 10*(1), 193–203.

Perger, T., Wachter, L., Fleischhacker, A., & Auer, H. (2020). PV sharing in local communities: Peer-to-peer trading under consideration of the prosumers' willingness-to-pay. *Sustainable Cities and Society, 66*, Article 102634.

Phommixay, S., Doumbia, M. L., & Qiushi, C. (2021). A two-stage two-layer optimization approach for economic operation of a microgrid under a planned outage. *Sustainable Cities and Society, 66*, Article 102675.

Pourbehzadi, Motahareh, Niknam, Taher, Aghaei, Jamshid, Mokryani, Geev, Shafie-khah, Miadreza, & Catalão, João P. S. (2019). Optimal operation of hybrid AC/DC microgrids under uncertainty of renewable energy resources: A comprehensive review. *International Journal of Electrical Power & Energy Systems, 109*, 139–159.

Rostami, M.-A., Kavousi-Fard, A., & Niknam, T. (2015). Expected cost minimization of smart grids with plug-in hybrid electric vehicles using optimal distribution feeder reconfiguration. *IEEE Transactions on Industrial Informatics, 11*(2), 388–397.

Sadaei, Hossein Javedani, Silva, Petrônio Cândido de Lima e, Guimarães, Frederico Gadelha, & Lee, Muhammad Hisyam (2019). Short-term load forecasting by using a combined method of convolutional neural networks and fuzzy time series. *Energy, 175*, 365–377.

Subhash, B., & Rajagopal, V. (2014). Overview of Smart metering system in Smart Grid scenario. March. In *2014 Power And Energy Systems: Towards Sustainable Energy* (pp. 1–6).

Ur-Rehman, O., Zivic, N., & Ruland, C. (2015). Security issues in smart metering systems. In *2015 IEEE International Conference on Smart Energy Grid Engineering (SEGE)* (pp. 1–7). https://doi.org/10.1109/SEGE.2015.7324615

Werbos, P. J. (1990). Backpropagation through time: What it does and how to do it. *Proceedings of the IEEE, 78*(10), 1550–1560.